25th ABCM International Congress of Mechanical Engineering
October 20-25, 2019, Uberlândia, MG, Brazil

COB-2019-1415
TIME DOMAIN RESPONSE OF HELMHOLTZ RESONATORS UNDER LINEAR AND NONLINEAR EXCITATION IN SUBSONIC FLOW

Emerson A. Camargo
Roberto F. Bobenrieth Miserda
Marcus V. G. de Morais
Adriano T. Fabro
Department of Mechanical Engineering, University of Brasilia, Brasilia, DF, 70910-900, Brazil
emerson.almeidac@gmail.com, rfbm@unb.br, mvmorais@unb.br, fabro@unb.br

Abstract. *Helmholtz resonators play an important role in acoustic treatment nowadays. Typically, turbofans use acoustic liners, that can be described as arrays of Helmholtz resonators. Current trends for the next generation of turbofans engines are towards higher bypass ratio, aiming better efficiency and lower noise along with increased distances between the fan and the outlet guide vanes. Commonly placed at intakes and bypass ducts, liners can also be used in the interstage region. However, in this region, the liner is subjected to a swirl component associated with strong nonlinear effects, which can significantly decrease its acoustic performance. In this work, a numerical approach is proposed to investigate the acoustic interaction of a lined array of resonators when subject to subsonic flow and high amplitude pressure sources. The simulations were carried out with the Virtual Aeroacoustic Tunnel (VAT), an in-house code developed at Computational Aeroacoustic Laboratory (CAALab) of University of Brasilia, in which the Euler's equations are used to simulate compressible inviscid transient flow with the immersed boundary method. Three test cases including a simple duct with flow and source, a lined duct with flow and also a lined duct with flow and source are proposed. The results show the time and frequency domain response for different operational conditions. Simulations of a duct with no liner show the potential of the proposed numerical approach for generating plane waves. Moreover, a numerical model including a lined duct configuration, i.e. a periodic array o resonators symmetrically distributed, shows the resulting aeroacoustic field due to the interaction of the subsonic flow with the resonators and also due to the subsonic flow with the presence of a distributed pressure source. The obtained results show that the proposed approach can effectively simulate nonlinear response due to the source excitation and interaction with the liners and thus can be applied for further investigation.*

Keywords: *Helmholtz resonator, acoustic liner, Virtual Aeroacoustic Tunnel, Euler equations*

1. INTRODUCTION

Helmholtz resonators became standard for the aircraft industry in control of excessive turbofan engine inlet/exhaust noise (Hersh *et al.*, 2003). According to Tam *et al.* (2008) acoustic liner, that is an array of Helmholtz resonators, is one of the most effective means to suppress jet engine fan noise.

Melling (1973) recognized the dependence of liner behavior with the incident sound pressure level (SPL): depending on the SPL, the liner can behave linearly or nonlinearly. Further, experiment shows that liner performance is affected by airflow over its surface and it is possible that both effects are interdependent. According to Tam and Kurbatskii (2000) in the linear regime, the flow at the resonator's neck is linear and the dissipative and resistive losses are due to the viscous dissipation, whereas in nonlinear case a turbulent jet can be observed and are the primary mechanism of dissipation.

Current trends for the next generation of turbofans engines are towards higher bypass ratio, aiming better efficiency and lower noise along with increased distances between the fan and the outlet guide vanes. These trends mean, however, higher nacelles diameters with increased drag, thus introducing the need for a reduction in the length of the nacelle. Commonly placed at intakes and bypass ducts, liners can also be used in the interstage region. However, in this region, the liner is subjected to a swirl component associated with strong nonlinear effects, which can significantly decrease its acoustic performance. The consequences of this scenario are the overall reduction of lined surfaces areas as well as the increase in the relative importance of the interstage liner.

This paper aims at simulating the time domain response of Helmholtz resonators arranged in a liner configuration and under nonlinear excitation in subsonic flow. The obtained results show that the methodology used was effective in simulating the response of liner to a subsonic flow and nonlinear pressure excitation.

Section 2. presents a brief summary of the numerical methodology used in this work. Section 3. presents the obtained numerical results and discussion. Finally, Section 3. presents some concluding remarks and further steps of the work.

2. NUMERICAL METHODOLOGY

The present work uses the Virtual Aeroacoustic Tunnel(VAT), a source-code developed at Computational Aeroacoustic Laboratory (CAALab) of University of Brasilia (Pimenta and Miserda, 2019). In order to simulate a compressible inviscid transient flow, the Euler's equations are used. Equations for continuity, momentum in the x-direction, momentum in the y-direction and energy, i.e.

$$\frac{\partial \rho}{\partial t} + \nabla \cdot (\rho \mathbf{V}) = 0, \tag{1}$$

$$\frac{\partial (\rho u)}{\partial t} + \nabla \cdot (\rho u \mathbf{V}) = -\frac{\partial p}{\partial x} + f_x, \tag{2}$$

$$\frac{\partial (\rho v)}{\partial t} + \nabla \cdot (\rho v \mathbf{V}) = -\frac{\partial p}{\partial y} + f_y, \tag{3}$$

$$\frac{\partial (\rho e_T)}{\partial t} + \nabla \cdot (\rho e_T \mathbf{V}) = -\nabla \cdot (p \mathbf{V}) + \mathbf{f} \cdot \mathbf{V}, \tag{4}$$

where ρ is density, u is the x-component velocity, v is the y-component velocity, $\mathbf{V} = u\hat{\imath} + v\hat{\jmath}$ is the velocity, p is the pressure, e_T is the total energy, f_x is the x-component field force, f_y is the y-component field force, $\mathbf{f} = f_x\hat{\imath} + f_y\hat{\jmath}$ is the field force and t is time. There are five unknowns in this system of equations, namely, density (ρ), x-component velocity (u), y-component velocity (v), pressure (p) e total energy (e_T). In order to make it consistent, two new equations can be added

$$e_T = e + \frac{\mathbf{V}^2}{2} = e + \frac{u^2 + v^2}{2}, \tag{5}$$

$$p = \rho e(\gamma - 1), \tag{6}$$

where e is the internal energy and γ is the heat capacity ratio. Then, the system is consistent with six equations for six unknowns. Equations 1 to 4 can be written in more compact vectorial notation, that will be useful in the discretization

$$\frac{\partial \mathbf{U}}{\partial t} + \nabla \cdot \Pi = \mathbf{R}, \tag{7}$$

where

$$\mathbf{U} = \begin{pmatrix} \rho \\ \rho u \\ \rho v \\ \rho e_T \end{pmatrix}, \Pi = \begin{pmatrix} \rho u & \rho v \\ \rho u u + p & \rho v u \\ \rho u v & \rho u v + p \\ (\rho e_T + p)u & (\rho e_T + p)v \end{pmatrix}, \mathbf{R} = \begin{pmatrix} 0 \\ f_x \\ f_y \\ f_x u + f_y v \end{pmatrix}, \tag{8}$$

were $\mathbf{U}$ is the vector of variables, Π is the flux tensor and $\mathbf{R}$ is the vector of body forces. In this method, the domain is discretized in finite volumes. Two basic approximations are considered since the volume is sufficiently small. First, the properties are constant over a control volume. Second, the properties over the surfaces are constant also. Hence, Eq. 7 is integrated over each single control volume and divided by its volume, making a spatial mean of the equation over the volume, yielding

$$\frac{\partial}{\partial t}\left(\frac{1}{V}\int_V \mathbf{U} dV\right) = -\frac{1}{V}\int_V (\nabla \cdot \Pi) dV + \left(\frac{1}{V}\int_V \mathbf{R} dV\right). \tag{9}$$

The term between parenthesis in Eq. 9 are the definitions of the volumetric mean of $\mathbf{U}$ and $\mathbf{R}$, called, respectively, $\overline{\mathbf{U}}$ and $\overline{\mathbf{R}}$. The first term of right-hand side equation, relative to de divergence of the tensor of flux, can be rewritten from the volume integral to a surface area integral using Gauss's flux theorem, what leads Equation 9 to

$$\frac{\partial \overline{\mathbf{U}}}{\partial t} = -\frac{1}{V}\int_S (\Pi \cdot \mathbf{n}) dS + \overline{\mathbf{R}}, \tag{10}$$

where S is the area and $\mathbf{n}$ is the normal vector related.

Equation 10 is valid to all of the control volumes, in any kinds and shapes. The VAT code, however, uses a regular Cartesian mesh, that is a square in two-dimensional case. Figure 1 illustrates a generic control volume (i, j) in a Cartesian mesh. The left side of the figure shows the control volume painted in blue, the surfaces delimiting the volume in red and the normals related to each surface in green.

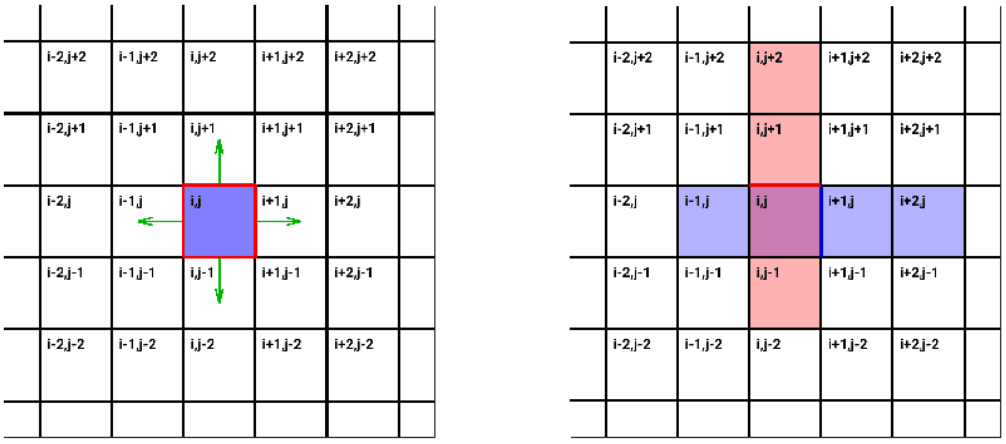

Figure 1. Schematic representation of VAT Cartesian mesh. (Left) Control volume (light blue) with surfaces (red) and normals (green). (Right) Example of stencil used for surface interpolation (blue for right surface and red for top surface).

For this specific control volume, with this geometry, equation 10 can be written as

$$\frac{\Delta \overline{\mathbf{U}}_{i,j}}{\Delta t} = -\frac{1}{V_{i,j}}\left[(\Pi \cdot \mathbf{S})_{i+\frac{1}{2}} + (\Pi \cdot \mathbf{S})_{i-\frac{1}{2}} + (\Pi \cdot \mathbf{S})_{j+\frac{1}{2}} + (\Pi \cdot \mathbf{S})_{j-\frac{1}{2}}\right] + \overline{\mathbf{R}}_{i,j}. \tag{11}$$

From Equation 10 to 11, the time derivative was discretized and the integral term was replaced by a sum. The sub-indexes $i+\frac{1}{2}$, $i-\frac{1}{2}$, $j+\frac{1}{2}$, $j-\frac{1}{2}$ indicates, respectively, right, left, top and bottom faces of volume (i, j). Equation 11 can be yet rewritten as

$$\Delta \overline{\mathbf{U}}_{i,j}, = -\mathcal{F}_{i,j} + \mathcal{R}_{i,j}, \tag{12}$$

where

$$\mathcal{F}_{i,j} = \frac{\Delta t}{V_{i,j}}\left[(\Pi \cdot \mathbf{S})_{i+\frac{1}{2}} + (\Pi \cdot \mathbf{S})_{i-\frac{1}{2}} + (\Pi \cdot \mathbf{S})_{j+\frac{1}{2}} + (\Pi \cdot \mathbf{S})_{j-\frac{1}{2}}\right], \tag{13}$$

$$\mathcal{R}_{i,j} = \Delta t \cdot \overline{\mathbf{R}}_{i,j}. \tag{14}$$

Equation 11 tells that the change of vector $\overline{U}$ after a time step Δt is related to two different sources, namely the flux of the properties through the surface $(\Pi \cdot \mathbf{S})$ and the body force acting over the control volume $(\overline{\mathbf{R}})$. To calculate each property in the surface, VAT uses a scheme that consists in the interpolation of two control volumes ahead and two behind the surface, for example

$$f_{i+\frac{1}{2},j} = \frac{9}{16}\left(\overline{f}_{i,j} + \overline{f}_{i+1,j}\right) - \frac{1}{16}\left(\overline{f}_{i-1,j} + \overline{f}_{i+2,j}\right), \tag{15}$$

$$f_{i,j+\frac{1}{2}} = \frac{9}{16}\left(\overline{f}_{i,j} + \overline{f}_{i,j+1}\right) - \frac{1}{16}\left(\overline{f}_{i,j-1} + \overline{f}_{i,j+2}\right), \tag{16}$$

where f can be any property of vector $\mathbf{U}$, in equation 8. The right image in Figure 1 shows an example of the stencil utilized for surface calculation. Equation 15 is illustrated in blue and equation 16 in red. The body force here is a inertial force used to accelerate the flow. At first, VAT imposes initial thermodynamic conditions over all computational domain for a stationary mass of air, then uses a inertial force to start the flow and accelerate it to the pre-set velocity.

For numerical stability of the code and control of numerical error caused by strong derivatives, VAT uses an artificial dissipation based in some sensors. The equation 12 becomes

$$\Delta\overline{\mathbf{U}}_{i,j} = -\mathcal{F}_{i,j} + \mathcal{R}_{i,j} + \mathcal{D}_{i,j}. \tag{17}$$

The calculation of $\mathcal{D}_{i,j}$ uses dissipation for each face, and these dissipations are proportional to the velocity field rotational, velocity field divergent, pressure gradient and density gradient.

For boundary conditions, VAT uses an immersed-boundary method, that consists of apply boundary conditions into the control volumes where the points of geometry lay on. The imposed conditions for boundary are of null derivatives in the normal direction:

$$\frac{\partial\rho}{\partial x_n} = \frac{\partial\mathbf{u}}{\partial x_n} = \frac{\partial p}{\partial x_n} = 0. \tag{18}$$

The directional derivatives of a property f can be calculated as the projection of the gradient of this property in the direction $\mathbf{n}$, what leads

$$\frac{\partial f}{\partial x_n} = \nabla f \cdot \mathbf{n} = n_x\left(\frac{\partial f}{\partial x}\right) + n_y\left(\frac{\partial f}{\partial y}\right) \tag{19}$$

To calculate these derivatives, a progressive scheme of finite differences is used. For instance, the x-derivative is given as

$$\left(\frac{\partial f}{\partial x}\right)_{i,j} = \frac{1}{12\Delta x}\left(-25f_{i,j} + 48f_{i+1,j} - 36f_{i+2,j} + 16f_{i+3,j} - 3f_{i+4,j}\right) + O(\Delta x)^4 \tag{20}$$

Consequently, it is possible to calculate the value that property f must assume in the boundary volume control to make null the derivative

$$f_{i,j} = \frac{1}{25}\left(48f_{i+1,j} - 36f_{i+2,j} + 16f_{i+3,j} - 3f_{i+4,j}\right) + O(\Delta x)^4, \tag{21}$$

$$f_{i,j} = D_i^+ f + O(\Delta x)^4. \tag{22}$$

The same rationale can be applied to the y-direction

$$f_{i,j} = D_j^+ f + O(\Delta y)^4, \tag{23}$$

and finally, for a boundary control volume,

$$f_{i,j} = \frac{|n_x|D_i^+ f + |n_y|D_j^+ f}{|n_x| + |n_y|}. \tag{24}$$

Figure 2 illustrates the immersed-boundary method. The black dots are surface points and the black arrows are the normals. The green control volumes are those that contain surface points. Is given an example of the stencil used for one control volume and the green arrow is the normal vector in this surface point, yellow is relative to x-component (equation 22) and blue is relative to y-component (equation 23).

The Cartesian mesh is composed of a regular region and by a stretched region. The regular region is a rectangle where the geometry is inserted and where is the interest of simulation. The stretched region, however, is necessary for giving a large amount of inertia to the fluid and represent a large field, where the waves can propagate.

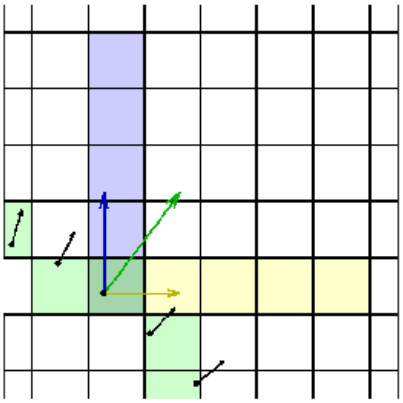

Figure 2. Illustration of immersed boundary method. The black dots are surface points and the black arrows are the normals. The green control volumes are those that contain surface points. The stencil used for one control volume and the green arrow is the normal vector in this surface point, yellow is relative to x-component and blue is relative to y-component.

3. NUMERICAL RESULTS

In this section, three numerical cases are presented. The first is a simple tube with flow and a distributed pressure source, the second is a lined duct only subjected to subsonic flow and, finally, the third introduces a distributed pressure source in the previous case. The visualization of results are made by two different manners: aeroacoustic field visualization and treatment of probes. For field visualization the variable $\beta_T = \sqrt[10]{\nabla T}$, is plotted. Pressure probes are visualized in time-domain and in the frequency domain.

3.1 Case 1: Flow and Source

The first geometry simulated is presented in Fig. 3, which shows the regular domain of simulation and where each unity in non-dimensional length is 2 mm long. The black dots indicate the rigid wall geometry, where are imposed the boundary conditions. The blue dots indicate the Isentropic Line Source, that works like a speaker. The pressure is imposed over a line in the wall and the other thermodynamic properties are imposed in order to generate a pressure variation that does not change entropy. Moreover, the green dots represent the probes where the values of pressure and velocity are measured. The geometry extends itself to left and to right until the end of the domain in order to simulate an infinite tube. The flow has Mach number $M = 0.6$, the tube has 92 mm of height and 800 mm of length in the regular domain.

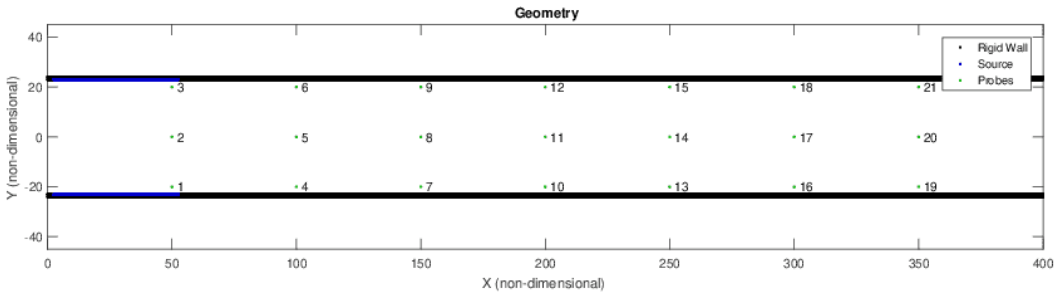

Figure 3. Regular domain for simulation. Simple tube to test generated waves.

This first geometry is used to demonstrate the generation of plane sound waves along the duct with pressure imposition at the wall. A sinusoidal signal of pressure is imposed over the distributed source with $12000Pa$ of amplitude at $2253Hz$. Figure 4 shows the time domain pressure signal measured at probe 26. This probe is positioned at the most downstream position among all probes. It also shows the corresponding frequency-domain Sound Power Level (SPL). Pressure spectrum shows the fundamental frequency and their harmonics.

Figure 5 shows the visualization of flow field. It is possible to see the plane waves (bright vertical lines) generated by

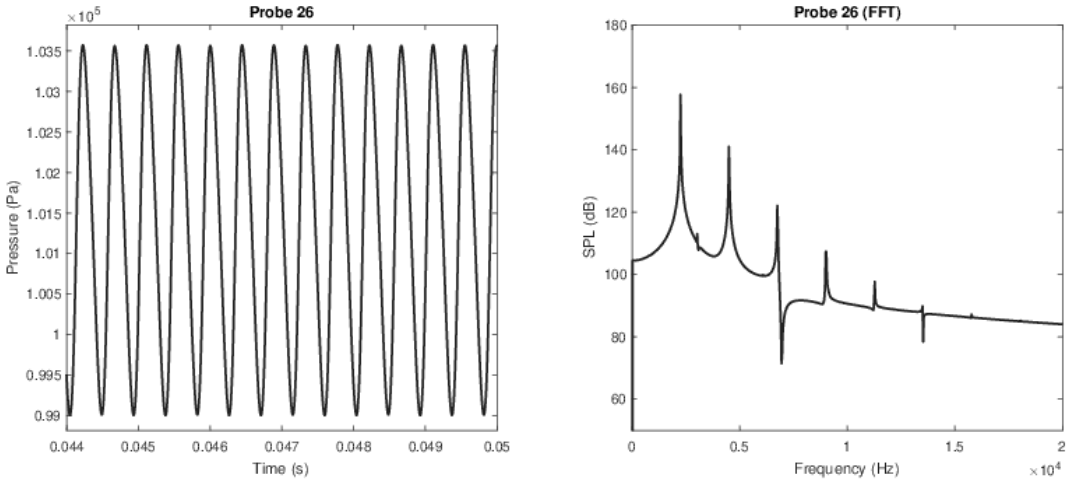

Figure 4. Pressure signal and spectrum of probe 26.

distributed source (dark horizontal lines).

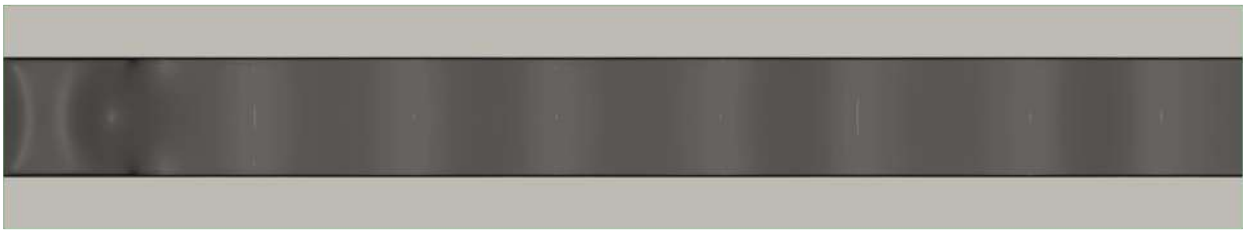

Figure 5. Field visualization with β_T

3.2 Case 2: Flow and Liner

The second geometry considered is presented in Fig. 6, which shows the whole regular domain for this simulation. The black dots indicate the rigid wall. The fluid is accelerated to the right direction until $Mach = 0.6$ with no pressure imposition at the wall. In addition, Figure 7 presents a detail view of some resonators in this liner.

The aim of this case is to study the behaviour of this liner under a flow with high velocity. Fig. 8 presents the visualization the obtained aeroacoustic field. The presence of liners generates a system of strong waves that propagates upstream with two evident types of waves: a plane waves and a x-wave. Figure 9, shows the time and frequency domain response at probe 2. Time domain signal shows an intense response, with high-amplitude ($10kPa$) sound waves that are almost discontinuous. Pressure spectrum shows that the dominant frequency is 2253 Hz.

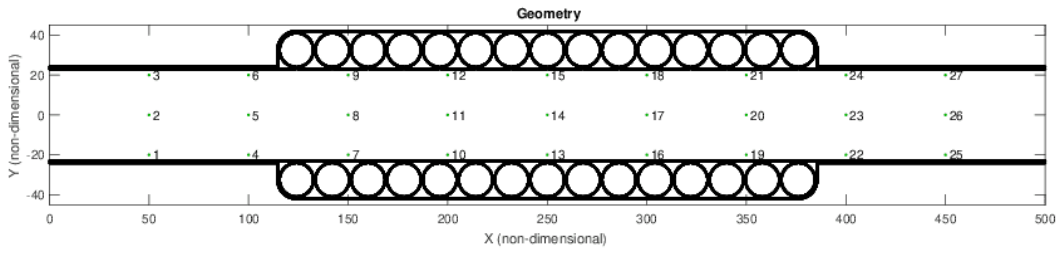

Figure 6. Regular domain of the lined duct.

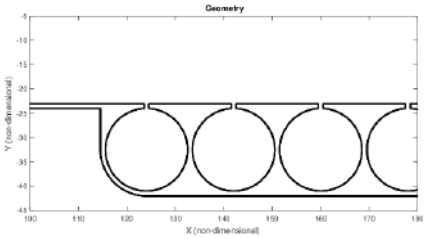

Figure 7. Detailed visualization of liner geometry.

Figure 8. Field visualization with β_T of the lined duct subjected to a subsonic flow.

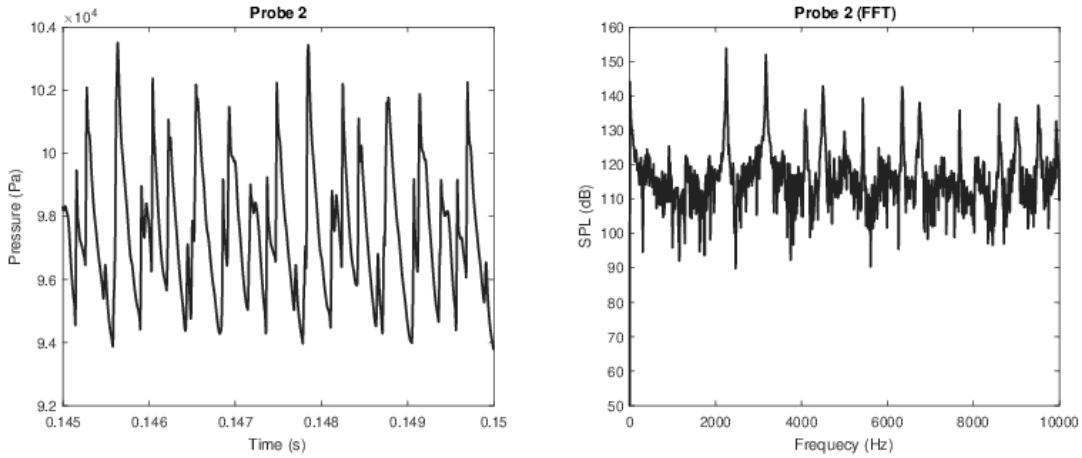

Figure 9. (left) The obtained time domain pressure signal and (right) SPL spectrum at probe 2.

3.3 Case 3: Flow, Source and Liner

This simulation case aims to study the acoustic response of the lined duct subjected to flow and an isoentropic line pressure source. The geometry of this case, Fig. 10 is the same as in Case 2. The blue lines represent the source.

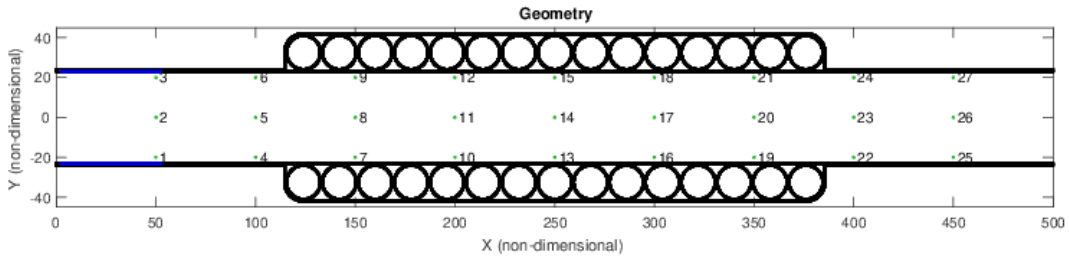

Figure 10. Regular domain for case 3 simulation with the geometry of the rigid wall (black lines) the isoentropic pressure source (blue lines) and the measurement probes (green dots).

Figure 11 presents the aeroacoustic field obtained. It is interesting to notice that there is a difference in the generated wave system caused by the presence of the source: in this case, the x-waves are clearly weaker when compared to the previous case.

Figure 11. Field visualization with β_T

4. CONCLUDING REMARKS

This work has presented a numerical investigation of the time domain response of Helmholtz resonators arranged in a liner configuration and under nonlinear excitation in subsonic flow. The simulation was carried out using the CAALab-VAT developed at the University of Brasilia using the immersed boundary method. Results showed nonlinear behavior of high-pressure waves as well in liner response of liner's response. This proves that the methodology is capable of simulating the nonlinearities and can be used for further investigation. Further steps include investigating the influence of velocity in the nonlinearity of the liner's response and the effects of different sound pressure levels of excitation.

5. ACKNOWLEDGEMENTS

The authors would like to acknowledge CAPES and CNPq for the financial support.

6. REFERENCES

Hersh, A.S., Walker, B.E. and Celano, J.W., 2003. "Helmholtz resonator impedance model, part 1: Nonlinear behaviour". *AIAA Journal*, Vol. 41, No. 5, pp. 795–808.

Melling, T.H., 1973. "The acountic impedance of perforates at medium and high sound pressure levels". *Journal of Sound and Vibration*, Vol. 29, No. 1, pp. 1–65.

Pimenta, B.G. and Miserda, R.F.B., 2019. "Numerical Simulation of Multiple Pure Tone Noise Generated by Supersonic Rotor Cascades". *Journal of Propulsion and Power*, Vol. 35, No. 3, pp. 530–543. doi:10.2514/1.B37216.

Tam, C.K.W., Ju, H. and Walker, B.E., 2008. "Numerical simulation of a slit resonator in a grazing flow under acoustic excitation". *Journal of Sound and Vibration*, Vol. 313, No. 1, pp. 449–471.

Tam, C.K.W. and Kurbatskii, K.A., 2000. "Microfluid dynamics and acoustics of resonant liners". *AIAA Journal*, Vol. 38, No. 8, pp. 1331–1339.

7. RESPONSIBILITY NOTICE

The authors are the only responsible for the printed material included in this paper.